Materials Letters 346 (2023) 134473

Contents lists available at ScienceDirect

Materials Letters

journal homepage: www.elsevier.com/locate/matlet

# Enhanced wear and corrosion resistances of Al coated Mg alloy using high pressure cold sprayed commercially pure-zirconium coating

M. Daroonparvar [a,d,*], A. Helmer [b], A.M. Ralls [a], M.U. Farooq Khan [b,c], A.K. Kasar [a], P.L. Menezes [a], M. Misra [d], R.K. Gupta [b]

[a] Department of Mechanical Engineering, University of Nevada, Reno, NV 89501, USA
[b] Department of Materials Science and Engineering, College of Engineering, North Carolina State University, 911 Partners Way, Raleigh, NC 27695, USA
[c] Department of Nuclear Engineering, Texas A&M University, College Station, TX 77843 USA
[d] Department of Chemical and Materials Engineering, University of Nevada, Reno, NV 89501, USA

ARTICLE INFO

*Keywords:*
Mg alloy
Metallic coating
Corrosion
Tribological performance

ABSTRACT

Commercially pure (CP) Zr coating with high microhardness (387 ± 26 $HV_{0.025}$) was produced on CP-Al coated Mg alloy by a high pressure cold spray (HPCS) system. Substantial densification of Al layers, beneath deposited Zr coating, was observed because of shot-peening influence by Zr particles. The electrochemical impedance spectroscopy after 24 h of immersion in 3.5 wt% NaCl electrolyte revealed highest charge transfer resistance ($R_{ct}$), polarization resistance ($R_{pol}$), and corrosion resistance ($|Z|_{f=0.01Hz}$) for the Zr/Al coated Mg alloy. Also, wear rate for the Zr/Al coating was lowest which could be attributed to its higher hardness caused by smaller crystallite size and higher dislocation density.

## 1. Introduction

Because of various advantages [1], surface modification of Mg alloys with the cold sprayed (CS) metallic coatings has recently received considerable attention over other processes [1–4]. Al-based coatings have been reported to improve properties of Mg alloys [1]. In fact, there is less increase in the density of the Mg alloy substrates when Al is used as coating [1]. However, Al and Al-based alloys because of their low wear resistance and relatively low corrosion resistance can't be extensively employed as mono layer CS noble barrier coatings on Mg alloys [5]. Tribological performance of CS Al coatings has been described to improve when hard-ceramic particles are added into the Al feedstock [6]. However, interface between Al and ceramic particles was noticed to act as quick channels for the corrosive electrolyte permeation [6]. Multilayered materials consisting of a CS Ti coating on Al in lieu of bulk Ti has been recently introduced [7]. Multilayered materials strategy created a balance between cost reduction and greater surface properties of Ti [7]. Ti, Hf, and Zr (from group 4B) have excellent resistance to corrosion and low standard reduction potential mismatch with Al and Mg [8]. In this study, CP-Zr coating with high microhardness was achieved on CP-Al coated Mg alloy. The microstructures, electrochemical corrosion behavior and tribological performance of coated Mg alloys were then investigated and discussed.

## 2. Materials and methods

CP–Al powder and CP-Zr powder were employed as feedstock powders. Substrate was machined from commercially available AZ31B Mg alloy plate. Mg alloy surface was prepared and then coated with metallic powders by a HPCS system (supplementary information (S1)). Optical microscopy, X-ray diffraction analysis, optical profilometry, Vickers microhardness tests, and dry reciprocating sliding tests using Rtec Tribometer at room temperature (S1) were employed to characterize the samples. As for electrochemical corrosion tests, the electrochemical impedance spectroscopy tests were implemented up to 24 h in 3.5 wt% NaCl electrolyte (S1).

## 3. Results and discussion

The microstructure of as- sprayed coatings cross-section on Mg-based alloys at various magnifications and schematic illustration of coatings formation are shown in Fig. 1a-1i. The porosity level of 0.133 ± 0.034% was obtained for the CS Al coating after applying the CS Zr top coating with porosity level of 0.246 ± 0.088% (Fig. 1a-1c). Highly deformed

* Corresponding author at: Department of Mechanical Engineering, University of Nevada, Reno, NV 89501, USA.
*E-mail address:* mr.daroonparvar@yahoo.com (M. Daroonparvar).

https://doi.org/10.1016/j.matlet.2023.134473
Received 13 December 2022; Received in revised form 20 April 2023; Accepted 28 April 2023
Available online 2 May 2023

inter-particle boundaries with tight bonding (Fig. 1d) and a significant work/strain hardening in the microstructure of CS coating [9] are expected due to severe plastic deformation of Zr particles upon impact with a surface. Besides the penetration of Zr top coating into Al layer and formation of extruded lips (Fig. 1a-1c), the substantial densification of the beneath deposited Al layers (owing to shot peening influence) by Zr particles (having a great kinetic energy) is apparent compared to the mono layer CP-Al coating on Mg alloy (with 0.203± ± 0.043%% porosity level), Fig. 1e-1 h. This phenomenon was reported when hard powder particles (with a high kinetic energy) impacted the soft substrate surface [9]. Both feedstock powders and CS coatings depicted the same phases and crystalline planes (Fig. 1j and 1 K). Compared to previous studies on Zr coatings/deposits [10,11], no phase transformation, oxidation and zirconium hydride precipitate formation were seen in the resultant CS coatings. The Williamson-Hall (W-H) method was employed to ascertain the average crystallite size and microstrain from the XRD fitting curves (Fig. 1l and 1 m). Microstrain (ε) is mostly stimulated by dislocations [12]. The average dislocation density was higher for Zr coating in comparison with that of Al coating (Table 1, equation. 2 (S1)). Compared to CS Al coating (Fig. 1l), a steeper slope of the W-H plot for Zr coating shows this coating contains a large amount of microstrain caused by severe plastic deformation (Table 1). In fact, the existence of crystal defects (especially dislocations) that are formed during CS process cause this microstrain in the structure. The existence of smaller crystallites and a considerable microstrain were attributed to the sub-grains formation in the severely deformed microstructure of the individual deformed particle in the CS coating structure [13].

The Nyquist and Bode plots of samples after 24 h immersion in 3.5 wt % NaCl solution are shown in Fig. 2a-2d. The impedance spectra were fitted using electrical equivalent circuits (EEC) depicted in Fig. 2e and 2f. In the EECs, capacitance (C) was replaced by the constant phase element (CPE or Q). The $R_{ct}$ value (as charge transfer resistance across electric double layer (as a phase boundary) at the interface between electrode and electrolyte) is proportionate to the reverse of the corrosion rate. The absolute impedances at low frequencies ($|Z|_{f=0.01Hz}$) (Fig. 2d) were used to determine the corrosion resistance of the samples [14,15]. The highest corrosion rate (lowest $R_{ct}$) and lowest polarization resistance at corrosion potential ($R_{pol}$) were obtained for the bare Mg alloy and compared to the coated samples (Table 2, supplementary information (S2)). Compared to Al coated Mg alloy in this research and Zr coated AZ91D Mg alloy in another research [8], Zr/Al coated Mg alloy demonstrated the maximum $|Z|_{f=0.01Hz}$ (or corrosion resistance) in 3.5% NaCl electrolyte, Fig. 2d. After spraying coatings on Mg alloy, bode phase plots (Fig. 2c) were markedly broadened (i.e., their aperture). This could be related to the protective capability of applied coatings on substrate [16]. In this regard, maximum phase angle near to − 80∘ (at a low-intermediate frequency) was observed for Zr/Al coated Mg alloy after 24 h.

After 24 h of immersion, the thickness of surface film (δ) on the CS Al and Zr/Al coatings was calculated (supplementary information (S3)) to

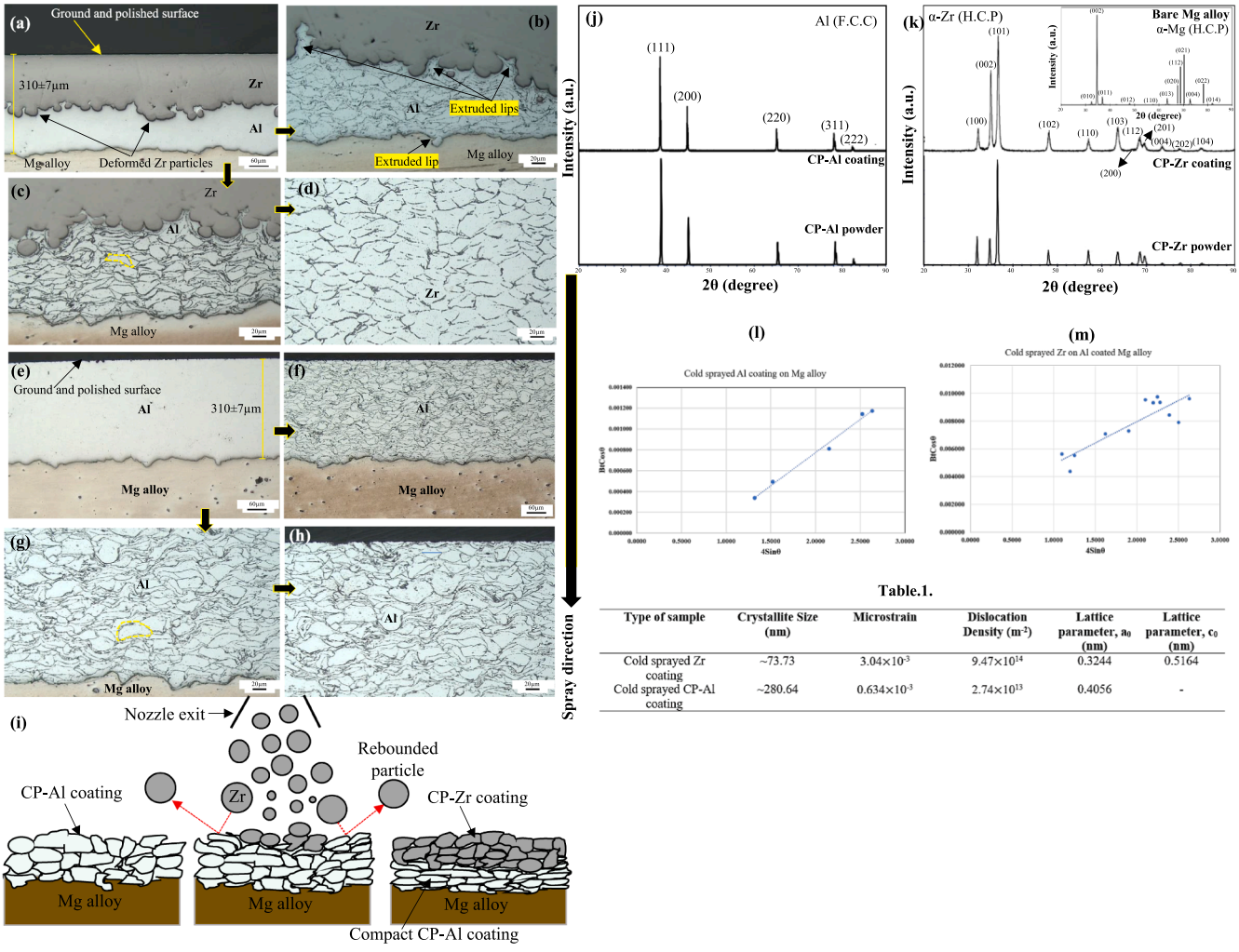


**Table.1.**

| Type of sample | Crystallite Size (nm) | Microstrain | Dislocation Density ($m^{-2}$) | Lattice parameter, $a_0$ (nm) | Lattice parameter, $c_0$ (nm) |
|---|---|---|---|---|---|
| Cold sprayed Zr coating | ~73.73 | $3.04\times10^{-3}$ | $9.47\times10^{14}$ | 0.3244 | 0.5164 |
| Cold sprayed CP-Al coating | ~280.64 | $0.634\times10^{-3}$ | $2.74\times10^{13}$ | 0.4056 | - |

**Fig. 1.** (a-h) photomicrographs of coatings cross section on Mg alloy, (i) schematic illustration of CS coatings formation on Mg alloy, (j, k) XRD patterns of feedstock powders and CS coatings, (l, m) W-H plots.

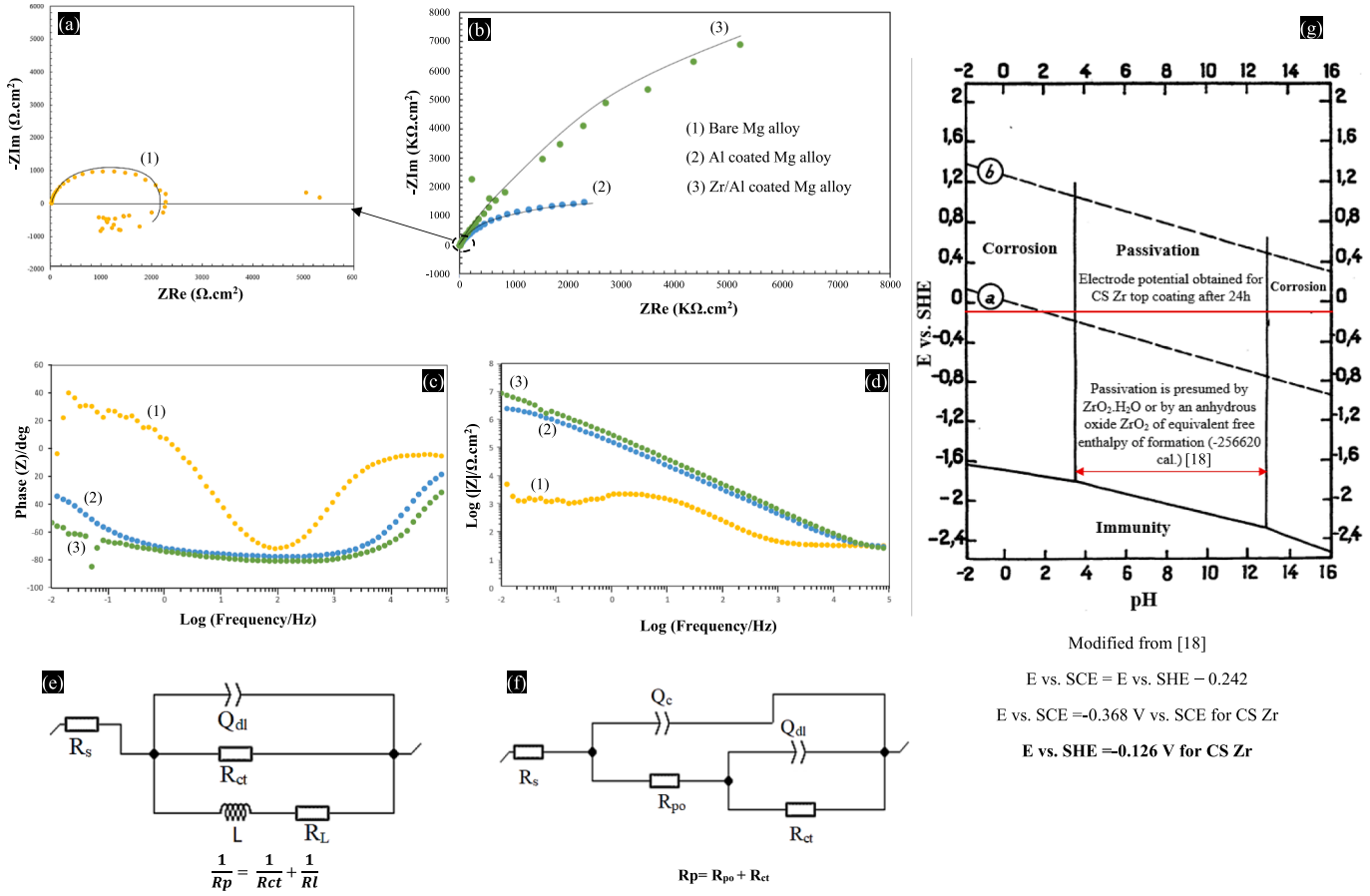


**Fig. 2.** (a-d) Nyquist and Bode plots of coated and bare Mg alloys, (e, f) used EECs, (g) E-pH diagram for Zr at 25 °C.

be 34.40 nm and 29.90 nm, respectively. The film capacitance ($C_c$) which was extracted from the film CPE ($Q_c$) was $3.44 \times 10^{-6}$ and $2.99 \times 10^{-6}$F.cm$^{-2}$ for CS Al and Zr/Al coatings, respectively. The higher film capacitance ($C_c$) was related to increased hydration of oxide layer ($Al_2O_3{\cdot}xH_2O$) in the course of immersion time. This was reported to enhance the $\varepsilon_\gamma$ value (S4) and finally lead to the reduction of corrosion

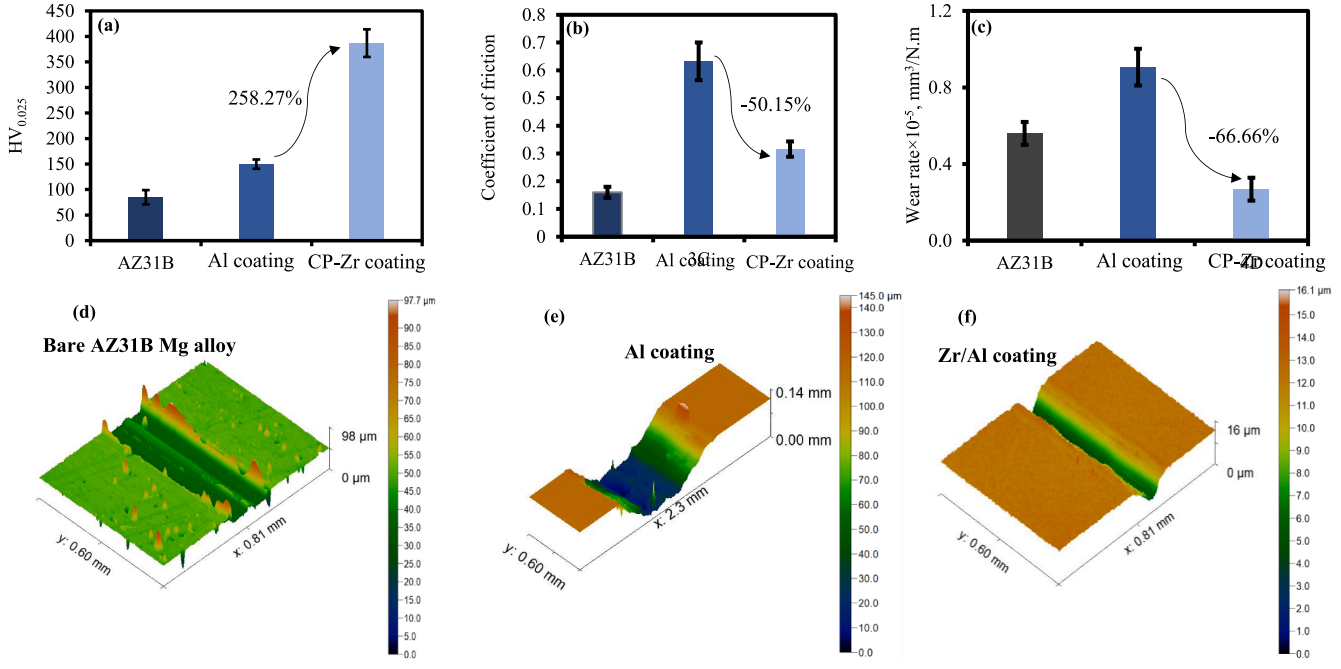


**Fig. 3.** (a-c) Microhardness, COF and wear rate of bare and coated Mg alloys, (d-f) wear tracks of bare and coated Mg alloys (3D surface profiles).

performance of Al [17].

In comparison with OCP value of bare Mg alloy (-1573 $mV_{SCE}$), the OCP values for Zr/Al and Al coated Mg alloys were −368 $mV_{SCE}$ and −839 $mV_{SCE}$, respectively after 24 h of immersion. This shows CS Zr coating on Al coated Mg alloy (having highest $R_{ct}$ and $|Z|_{f=0.01Hz}$) has the lowest tendency to corrode (from thermodynamic point of view) compared to the mono layer CS Al coating. According to the obtained potential (-368 $mV_{SCE}$) for Zr/Al coating and E-pH diagram for Zr (Fig. 2g, [18]), it can be postulated that the CS Zr coating is in the passivation region in most pH ranges even after 24 h. Severe plastic deformation of Zr particles upon severe impact can cause the considerable replication of dislocations, lattice microstrain stimulation, refined-crystals and more likely residual stresses in resultant CS coating structure (Table 1). In fact, the stored energy in the CS coatings is reported to assist the easy passivation [19].

The hardness value of Al coating was 150 ± 9 HV, whereas cold spraying Zr on Al coating increased hardness values to 387 ± 26 HV (Fig. 3a). As, classical Hall-Petch equation indicated that hardness goes up as crystallite size reduces [20]. Bare Mg alloy showed least coefficient of friction (COF) compared to that of CS coatings (Fig. 3b). This behavior was also reported by Siddique et al. [21]. Among the CS coatings, Zr/Al showed lesser COF ~ 0.3 compared to the CS Al coating. The lesser COF value of the Zr/Al is mainly due to the high hardness of the Zr top coating that reduced the ploughing component of friction compared to the CS Al coating. In fact, the increased hardness because of the remarkable plastic deformation in CS Zr coating structure (Table 1) could decrease the effective contact area between the ball and the wear track therefore decreasing frictional force [21].

The wear rate of the CS coatings showed a similar trend as observed in COF results of coated samples (Fig. 3b and 3c). The Zr/Al coating showed a lower wear rate compared to Al coating, which is due to its higher hardness. The depth of wear track for CS Zr top coating was appreciably lower than that of the other samples (Fig. 3d-3f). Although bare Mg alloy showed the least COF, the wear rate was higher than that of Zr/Al coating, which is also ascribed to the hardness values of these materials.

## 4. Conclusions

- Highest polarization resistance ($R_{pol}$) and $|Z|_{f=0.01Hz}$ were obtained for Zr/Al coated Mg alloy.
- Film thickness on CS coatings after 24 h of immersion was 34.40 nm for Al coating and 29.90 nm for Zr/Al coating.
- Zr/Al coating immersed for 24 h indicated a passive potential for a wide range of pHs.
- Lower wear rate obtained for Zr/Al coating was due to higher surface hardness caused by smaller crystallite size/higher dislocation density.

## Declaration of Competing Interest

The authors declare that they have no known competing financial interests or personal relationships that could have appeared to influence the work reported in this paper.

## Data availability

Data will be made available on request.

## Acknowledgment

RKG: National Science Foundation (NSF-CMMI 2131441) under the direction of Dr. Alexis Lewis.

## Appendix A. Supplementary data

Supplementary data to this article can be found online at https://doi.org/10.1016/j.matlet.2023.134473.

## References

[1] M. Daroonparvar, et al., J. Mag. Alloys 10 (2022) 2025–2061.
[2] Y. Zhou, et al., Mater. Letters 284 (2021), 128930.
[3] H. Yuan, et al., Materials Letters 289 (2021), 129389.
[4] M. Daroonparvar, et al., Vacuum 108 (2014) 61–65.
[5] Y.K. Wei, et al., Corrosion Sci 138 (2018) 105–115.
[6] N. Li, et al., Surf. Coat. Technol 349 (2018) 1069–1076.
[7] F. Rubino, et al, P. Cavaliere (Ed.), Cold-Spray Coatings., Springer, Cham (2017).
[8] D. Zhang, et al., Surf. Coat. Technol 303 (2016) 94–102.
[9] Z. Monette, et al., Int. J. Adv. Manuf. Technol. 106 (2020) 2079–2099.
[10] H. Sahasrabudhe, et al., Appl. Sci. 8 (2018) 393, https://doi.org/10.3390/app8030393.
[11] K.J. Hollis, et al., J Therm Spray Tech 21 (2012) 409–415.
[12] K. Maa, et al., Acta Mater 62 (2014) 141–155.
[13] W. Sun, et al., J. Alloys Comp. 797 (2019) 1268–1279.
[14] Z. Lia, Corrosion Sci 157 (2019) 295–304.
[15] A.V. Takaloo, et al., Mat. Sci. Appl 2 (2011) 1542–1555.
[16] R. Maurya, et al., Appl. Surf. Sci 443 (2018) 429–440.
[17] Z. Zhang, et al., Surf. Coat. Technol 370 (2019) 53–68.
[18] M. Pourbaix, Atlas of Electrochemical Equilibria in Aqueous Solutions, National Association of Corrosion, National Association of Corrosion; Second English Edition, 1974, p. P227.
[19] S. Kumar, et al., Surf. Coat. Technol 296 (2016) 124–135.
[20] D. Ali, et al., Physica B 444 (2014) 77–84.
[21] S. Siddique, et al., Surf. Coat. Technol 394 (2020), 125882.